Comprehensive Journal of Science
Volume (11), Issue (42), (Sapt, 2026)
ISSN: 3104-6266

مجلة العلوم الشاملة
المجلد (11) العدد 42 سبتمبر 2026
ردمد: 3104-6266

Energy and Exergy Performance of Crystalline Silicon and Perovskite Photovoltaic Modules in Sabratha, Libya: An Hourly Simulation Study

Fadia Khalifa Elghariani[1,*] and Abdulbaset Awsha[2]

[1] Department of Electrical and Electronic Technology, Higher Institute of Science and Technology, Sabratha, Libya

[2] Department of Electrical and Electronic Technology, Higher Institute of Science and Technology, Sabratha, Libya

*Corresponding author: fadiaelg208@gmail.com; co-author: abddulbasetushah@gmail.com

Received: 12/10/2026 Revised: 15/10/2026 Accepted: 02/11/2026 Publication: 26/11/2026

Abstract—This study asks whether the weak temperature dependence of a commercial-size, single-junction perovskite module offsets its lower nameplate efficiency relative to an n-type TOPCon crystalline-silicon (c-Si) module in Sabratha, Libya. Two hypothetical 100 MW_{dc} fixed-tilt arrays (33°, south-facing, ground coverage ratio 0.30), identical except for module properties, were simulated hourly in the System Advisor Model (SAM) with a satellite-derived NSRDB Meteosat typical meteorological year. Energy and exergy indicators were evaluated at the module boundary from nominal plane-of-array irradiance, modeled cell temperature, and gross DC power, using Petela's radiation exergy. In summer and winter, c-Si reached energy efficiencies of 18.96% and 19.86%, and perovskite 14.07% and 14.19%; approximate electrical exergy efficiencies were 20.4% and 21.3% for c-Si and 15.1% and 15.2% for perovskite. From winter to summer, c-Si energy efficiency fell by 4.5 relative percent, compared with 0.8 relative percent for perovskite. c-Si produced more gross DC energy per square metre of module, whereas the perovskite case produced about 5.4% more gross DC energy per installed kWp in summer and 1.7% more in winter. Under common irradiance and thermal assumptions, perovskite parity with c-Si would require a reference efficiency of about 20.2% in summer and 21.0% in winter. The results are model outputs that assume the perovskite efficiency and low-irradiance response, monofacial operation, and no degradation, and are unvalidated against measurements in Libya.

Index Terms—Exergy analysis, perovskite photovoltaics, TOPCon crystalline silicon, temperature coefficient, System Advisor Model, specific yield, Libya.

1. Introduction

Libya's southern regions receive roughly 2,100–2,500 kWh/m²/year of global horizontal irradiation (GHI) [1], yet its electricity supply depends almost entirely on oil and gas and suffers recurrent shortfalls [2], making photovoltaic (PV) generation a strategic option. The contrast between the Mediterranean coast and the desert interior also means that PV technologies should be assessed site by site rather than by extrapolating results from one location to the whole country [3], [4].

First-law efficiency quantifies how much incident solar energy becomes electricity, but not the quality of the energy streams. Second-law (exergy) analysis evaluates the work potential of the incident radiation and of each output and loss stream, separating useful electrical output from heat rejected near ambient temperature [5], [6]. Exergy studies of silicon modules show that the exergy efficiency depends on irradiance, ambient temperature, and module temperature [6], that it tends to be higher in the morning and late afternoon than at noon [7], and that field values vary widely with climate and module type [8], [9].

Metal-halide perovskites have advanced faster than any other PV absorber [10], and field studies indicate that their temperature response differs from that of silicon [11], [12], [13]. Libyan PV assessments have so far relied on energy and economic indicators [1], [2], [3], [4]. The present paper therefore compares an n-type tunnel-oxide passivated-contact (TOPCon) c-Si module and a modeled commercial-size perovskite module in Sabratha, on Libya's north-western coast, using hourly SAM

simulations and an independently computed energy and exergy model. The two arrays are hypothetical fixed-tilt design cases: only the weather inputs describe the site, and all performance quantities are model outputs.

2. Related Work and Research Gap

2.1. Energy and Exergy Assessment of PV Systems

A PV module is usually treated as a control volume that receives solar radiation, delivers electrical power (pure work, whose exergy equals its energy), and rejects heat. The exergy of the incident radiation is lower than its energy and depends on how radiation entropy is treated. Petela's expression [14] accounts for the entropy of black-body radiation emitted at an effective solar temperature and gives an exergy-to-energy ratio of about 0.93 near 25 °C. A simpler Carnot factor, $(1 - T_0/T_s)$, used in several PV studies [15], gives about 0.95. Joshi *et al.* [5] and Sarhaddi *et al.* [6] formulated exergy balances in which the heat rejected from the module surface is assigned an exergy content; Sarhaddi *et al.* also defined an exergy efficiency that subtracts this thermal exergy from the electrical exergy. That quantity is not a ratio of an output stream to the input, and Section 3.4 therefore treats it as a separately named indicator.

In a single-junction cell, substantial losses are intrinsic to the absorber: photons with energy above the bandgap lose their excess energy by carrier thermalization, and photons below the bandgap cannot generate power [16]. Together with Auger recombination, these mechanisms limit single-junction c-Si to about 29.4% [17]. A module-level simulation that does not resolve the spectrum cannot quantify these mechanisms, and the present study does not attempt to do so.

2.2. Temperature Response of TOPCon and Perovskite Modules

In a TOPCon cell, an n-type wafer with a boron-doped front emitter is contacted at the rear through an ultrathin silicon oxide (~1.4 nm) capped by phosphorus-doped polysilicon, which passes electrons while suppressing surface recombination; Feldmann *et al.* demonstrated 23.7% with this concept on a laboratory cell [18]. n-type wafers avoid boron–oxygen light-induced degradation and are less sensitive to metallic impurities [19], and TOPCon has become the dominant cell technology in global production [20]. The manufacturer's datasheet for the module adopted here specifies a power temperature coefficient of −0.30 %/°C [21]. Fig. 1(a) shows an illustrative cross-section of this cell type.

Perovskite cells place an $APbX_3$ halide absorber between electron- and hole-transport layers; in the inverted p–i–n configuration (Fig. 1(b)), light enters through a transparent conducting oxide and a hole-extraction layer, and composition tunes the bandgap over roughly 1.5–2.3 eV [16]. Under outdoor conditions, Velilla *et al.* observed relative advantages for perovskite at different irradiances [11], and Jošt *et al.* extracted a power temperature coefficient of −0.17 %/K for 1 cm² cells [12]. Ellis *et al.* monitored two commercial-size, glass–glass, single-junction perovskite modules of 0.7164 m² for one year at the European Solar Test Installation (northern Italy). They reported a maximum-power temperature coefficient of −0.054 %/°C at 1000 W/m² and a decrease of about 3 percentage points in efficiency over the year for the more stable module [13]. These Italian field measurements supply the perovskite module area and temperature coefficient used here; operation of that module in Libya is simulated, not measured.

2.3. Research Gap and Contributions

Exergy studies of PV modules have focused on silicon and Libyan studies on energy and economic indicators; to the authors' knowledge, no published study has compared c-Si and perovskite modules from an exergy perspective for a Libyan coastal site. Within that scope, the study contributes (i) a site-

specific hourly comparison of a TOPCon module and a commercial-size perovskite module whose temperature coefficient comes from one year of field characterization; (ii) explicit separation of the electrical exergy efficiency from a thermal-loss-adjusted indicator, with a defined control volume and an unallocated residual term; (iii) side-by-side area-based and capacity-based results that explain how each technology can lead on a different basis; and (iv) a conditional parity efficiency for the perovskite module, derived algebraically from the common modeling assumptions.

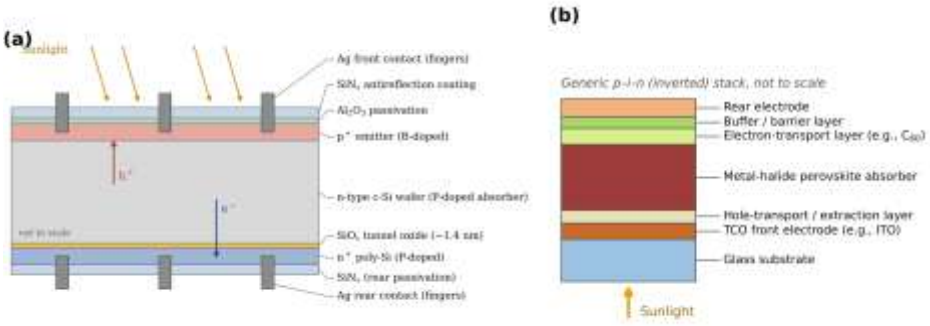

Fig. 1. Illustrative cell cross-sections (not to scale): (a) n-type TOPCon c-Si cell, drawn by the authors after [18], [19]; (b) generic inverted (p–i–n) perovskite stack, original schematic. Neither panel depicts the internal structure of the specific modules simulated.

3. Materials and Methods

3.1. Study Site and Typical Meteorological Year

Sabratha lies on the Mediterranean coast of north-western Libya, about 70 km west of Tripoli. Hourly weather data were taken from the typical meteorological year (TMY) product of the National Solar Radiation Database (NSRDB) derived from Meteosat Second Generation (MSG) satellite observations with the Physical Solar Model [22], [23]. The selected grid cell is centered at 32.81° N, 12.50° E, at an elevation of about 1 m. According to the source analysis, its TMY is composed of months drawn from 2015–2022. The product is distributed at 4 km and 60 min resolution [23]; the weather file itself was not available, so the source years and timestamp convention remain as reported. The annual GHI in the file is reported as 1,998 kWh/m²/year.

The analysis focuses on summer (June–August) and winter (December–February) as the two seasonal extremes. TABLE I summarizes the climatic conditions of each season. For the hourly analysis, the source study selected 17 July and 21 January as the clearest high-irradiation days of their seasons, with daily irradiation of 8.9 and 3.79 kWh/m²/day, respectively. The irradiance plane of these daily values (horizontal or plane-of-array) is not documented, and the two dates are treated here as illustrative cases rather than statistically representative days.

TABLE I. Seasonal climate at the selected grid point (NSRDB-MSG TMY, satellite-derived)

Variable	Summer (Jun–Aug)	Winter (Dec–Feb)
Mean daily GHI (kWh/m²/day)	7.61	3.36
Mean daily DNI (kWh/m²/day)	7.95	4.55
Mean daytime ambient temperature (°C)	28.4	15.6
Max./min. hourly ambient temperature (°C)	39.6 / 19.9	22.3 / 7.9
Mean wind speed (m/s)	3.87	5.17
Mean relative humidity (%)	63.3	68.5

3.2. PV Module Parameters and Array Configuration

Two hypothetical utility-scale arrays of 100 MW_{dc} each were defined; this is SAM's default utility capacity. The arrays share every input except the module (TABLE II). The c-Si case uses the Jinko JKM550N-72HL4-BDV, an n-type TOPCon module rated at 550 W_p [21]. The modeled reference efficiency of 21.32% follows from the nominal power and the rounded area of 2.58 m² (550 W / 2.58 m² = 213.2 W/m²); the datasheet lists 2278 × 1134 mm (2.583 m²) and an STC efficiency of 21.29% [21]. The difference of 0.03 percentage points comes from rounding the area. With 181,804 modules the DC capacity is 99.99 MW_{dc}. The irradiance-dependent efficiency table was derived from the CEC five-parameter single-diode model of the same module at 25 °C. The modeled temperature coefficient of −0.295 %/°C is the CEC-library input, whereas the manufacturer specifies −0.30 %/°C [21]. The manufacturer specifies this module as bifacial, glass–glass, with a bifaciality factor of 80 ± 5% [21], but both arrays were simulated as monofacial.

For the perovskite case, the module area of 0.7164 m² and the temperature coefficient of −0.054 %/°C (determined at 1000 W/m²) come from one year of outdoor measurements in northern Italy by Ellis *et al.* [13]. The reference efficiency of 15% and the flat irradiance–efficiency profile are modeling assumptions: the field study does not supply a nameplate efficiency or low-irradiance data. The 15% value is close to the 14.3% reported for a semitransparent perovskite module in [16]. With 107.46 W per module, 930,582 modules give 100.0 MW_{dc}.

TABLE II. Module and array inputs (external parameters and modeling assumptions)

Input	c-Si (TOPCon)	Perovskite
Module	Jinko JKM550N-72HL4-BDV [21]	Single-junction, commercial size [13]
Reference efficiency at 1000 W/m² (%)	21.32 modeled; 21.29 datasheet [21]	15.0 (modeling assumption)
Efficiency at 200/400/600/800 W/m² (%)	21.22/21.50/21.53/21.45 (CEC-derived)	15.0, flat (modeling assumption)
Power temperature coefficient γ (%/°C)	−0.295 modeled (CEC); −0.30 datasheet [21]	−0.054, measured in Italy [13]
Module area (m²) / rating (W)	2.58 modeled (2.583 datasheet) / 550	0.7164 [13] / 107.46 (derived)
Number of modules / DC capacity (MW_{dc})	181,804 / 99.99	930,582 / 100.0
Common inputs	Fixed tilt 33°, azimuth 180°, GCR 0.30, monofacial; 33 central inverters of 2.51 MW_{ac} (DC/AC = 1.21); soiling 5%; DC losses 4.44%; AC wiring 1%; Sandia glass/glass open rack a = −3.47, b = −0.0594 s/m, ΔT = 3 °C	

The 4.44% DC loss equals the combined SAM default for mismatch (2%), diodes and connections (0.5%), and DC wiring (2%): $1 - 0.98 \times 0.995 \times 0.98 = 0.0444$. It, inverter losses, clipping, and the 1% AC wiring loss lie downstream of gross DC power and affect only AC yield and PR, whereas soiling reduces the irradiance reaching the cells.

3.3. Hourly SAM Simulation and Temperature Model

Fig. 2 summarizes the workflow and the provenance of each data stream. SAM is a free, open-source performance and financial model [24], [25]. The simulations used SAM 2026.7.3 [24] with the Detailed PV model and, for both technologies, the Simple Efficiency Module Model. Using one module model for both cases ensures that differences arise from module parameters rather than from different model formulations. In the Simple Efficiency Module Model, gross module DC power is

$$P_{\mathrm{dc}} = \eta_{\mathrm{ref}}\, f(G_{\mathrm{eff}})\, [1 + \gamma(T_c - 25)]\, A\, G_{\mathrm{eff}} \tag{1}$$

where η_{ref} is the reference efficiency, f is the relative irradiance–efficiency profile ($f \equiv 1$ for the perovskite case), γ is the power temperature coefficient (1/°C), T_c is the cell temperature (°C), A is the total module area (m²), and G_{eff} is the effective plane-of-array (POA) irradiance after shading, soiling, and reflection losses (W/m²). Cell temperature follows the Sandia model [26]:

$$T_m = T_a + G\, e^{\,a+b\,v} \tag{2}$$

$$T_c = T_m + \frac{G}{G_0}\,\Delta T \tag{3}$$

where T_m is the module back-surface temperature (°C), T_a the ambient air temperature (°C), G the POA irradiance (W/m²), v the wind speed at the standard 10 m height (m/s), a and b empirical coefficients for the mounting and construction, G_0 = 1000 W/m², and ΔT the difference between cell temperature and module back-surface temperature at G_0 [26]. The glass/glass open-rack coefficients were applied to both arrays. Because (2)–(3) do not depend on conversion efficiency, the two arrays have identical modeled hourly cell temperatures.

TABLE III lists the quantities used, their source, and their position in the loss chain. Nominal POA irradiance G is evaluated after transposition but before shading, soiling, and reflection, whereas G_{eff} is evaluated after them and is the irradiance used in (1). Gross DC power is evaluated before DC losses, net DC after them, and grid-delivered AC energy after inverter and AC wiring losses. Because the SAM project and hourly exports were not available, the daylight mask and the handling of missing and low-irradiance hours cannot be recovered.

TABLE III. Quantities used, data type, units, and loss-chain stage

Symbol	Quantity	Type	Units	Stage
G	Nominal POA total irradiance	SAM output	W/m²	Before shading/soiling/reflection
G_{eff}	Effective POA irradiance	SAM internal	W/m²	After shading, soiling, reflection
T_a, v	Ambient temperature, wind speed	Satellite TMY	°C, m/s	Input
T_c	Cell temperature (Sandia)	SAM output	°C	Module
P_{dc}	Gross module DC power	SAM output	W	Before 4.44% DC losses
E_{AC}	Grid-delivered AC energy	SAM output	kWh	After inverter, clipping, 1% AC wiring
Ex_{in}, Ex_{th}, Ex_{res}	Exergy terms	Calculated	W; kWh	Module control volume

3.4. Energy Metrics, Solar Exergy, and System Boundary

The control volume is the module front surface, including its soiling layer, together with the module itself. Its radiative input is the nominal POA irradiance G over area A. Its outputs are gross DC electrical power and heat transferred to the surroundings. The dead state is the ambient air at the hourly temperature $T_0 = T_a + 273.15$ (K), and every thermodynamic ratio uses absolute temperature. Exergy rates are written with a dot and expressed in W; integrated exergy is written without a dot and expressed in kWh, for example $Ex_{in} = \Sigma_k\, \dot{E}x_{in,k}\, \Delta t$, where k indexes the hourly timestamps and Δt = 1 h. Numerators and denominators of all seasonal ratios are summed over the same set of daylight timestamps. The seasonal energy efficiency is

$$\eta_{en} = \frac{\sum_k P_{dc,k}\,\Delta t}{\sum_k G_k\, A\, \Delta t} \tag{4}$$

Following Petela [14], the exergy rate of the incident radiation is

$$\dot{E}x_{in} = G\, A \left[1 - \frac{4}{3}\frac{T_0}{T_s} + \frac{1}{3}\left(\frac{T_0}{T_s}\right)^4\right] \tag{5}$$

where T_s = 5777 K is the effective solar surface temperature. At T_0 = 298.15 K the bracketed factor is 0.931, compared with a Carnot factor of 0.948; efficiencies based on (5) are therefore slightly higher

than Carnot-based values. Electrical exergy equals gross DC power, $\dot{E}x_{el} = P_{dc}$. The exergy carried by convective heat transfer from the module surface to ambient air is evaluated at the cell temperature, a proxy for the surface temperature [5], [6]:

$$\dot{E}x_{th} = \left(1 - \frac{T_0}{T_c}\right) h_c A (T_c - T_0) \tag{6}$$

$$h_c = 5.7 + 3.8\, v \tag{7}$$

where T_c is in kelvin and h_c (W/m²·K) is a linear wind correlation [27]. Equation (6) is positive when $T_c > T_0$ and is counted as exergy leaving the control volume. It covers convection only. Longwave radiative exchange with the sky and ground, conduction to the mounting, and the reflected solar stream are not modeled separately. The exergy balance is therefore closed by a residual term:

$$\dot{E}x_{res} = \dot{E}x_{in} - \dot{E}x_{el} - \dot{E}x_{th} \tag{8}$$

Because G is nominal, the 5% soiling loss lies inside the boundary and within $\dot{E}x_{res}$, the unallocated exergy residual. It may also include reflection and shading losses, radiative and conductive heat exchange, the temperature-induced reduction of output, and cell conversion losses; the available results do not quantify these contributions separately. Two exergy indicators are formed from the integrated terms:

$$\psi_{el} = \frac{Ex_{el}}{Ex_{in}} \tag{9}$$

$$\psi_{adj} = \frac{Ex_{el} - Ex_{th}}{Ex_{in}} \tag{10}$$

The electrical exergy efficiency ψ_{el} is the ratio of the useful output to the input. The thermal-loss-adjusted indicator ψ_{adj} reproduces the formulation of [6] and of the source manuscript; it treats an exergy loss as a negative product, so it is a diagnostic indicator rather than an efficiency in the strict sense. Both are defined as ratios of seasonal sums. The source analysis published ψ_{adj} (17.04% and 17.77% for c-Si and 11.78% and 11.70% for perovskite in summer and winter; TABLE IV), and Fig. 3 plots ψ_{adj}. Because the hourly exports were not available, ψ_{el} could not be summed hour by hour. It is reconstructed approximately as η_{en} divided by the Petela factor of (5) evaluated at the seasonal mean daytime ambient temperature (0.9304 in summer and 0.9334 in winter), and is reported to one decimal place. As an internal consistency check, these reconstructions reproduce the Ex_{th}/Ex_{el} ratios published in the source to within 0.1 percentage points, which indicates that the published exergy values follow (10).

3.5. Aggregation, Normalization, and Break-Even Method

Area-normalized gross DC energy is $E_A = \Sigma P_{dc} \Delta t / A$ (kWh/m²). Capacity-normalized indicators follow IEC 61724-1 [28]:

$$Y_{DC} = \frac{E_{dc}}{P_0}, \quad Y_r = \frac{H_{POA}}{G_0}, \quad Y_f = \frac{E_{AC}}{P_0}, \quad PR = \frac{Y_f}{Y_r} \tag{11}$$

where P_0 is the installed DC capacity (kW_p), H_{POA} the POA irradiation (kWh/m²), and E_{dc} the gross DC energy. Y_{DC} is reported as gross DC specific yield; strictly, IEC 61724-1 defines the array yield on net DC output. PR is an AC metric.

For the parity (break-even) analysis, the c-Si case and a perovskite case with an unknown reference efficiency η^* are compared at equal area. Both receive the same G, so Ex_{in} per unit area is identical. Both have the same T_c under (2)–(3), so Ex_{th} per unit area is identical. Equal ψ_{adj} therefore requires equal Ex_{el}, which is also the condition for equal ψ_{el} and equal η_{en}. Under (1), with $f \equiv 1$ and identical T_c, perovskite DC power is proportional to η_{ref}. Hence

$$\eta^* = \eta_{ref,pvk} \frac{E_{A,cSi}}{E_{A,pvk}} = \eta_{ref,pvk} \frac{\eta_{en,cSi}}{\eta_{en,pvk}} \tag{12}$$

Under these common assumptions the exergy parity threshold is identical to an energy parity threshold. A loss that multiplies the effective irradiance of both arrays by the same constant factor cancels in (12), provided it does not change the technologies' relative responses or the weighting of hours. This cancellation is conditional: because the c-Si efficiency depends on G_{eff} (TABLE II) while the perovskite profile is flat, a different soiling level shifts c-Si along its efficiency curve, and seasonally varying soiling reweights the hours. Either effect could change η^* slightly.

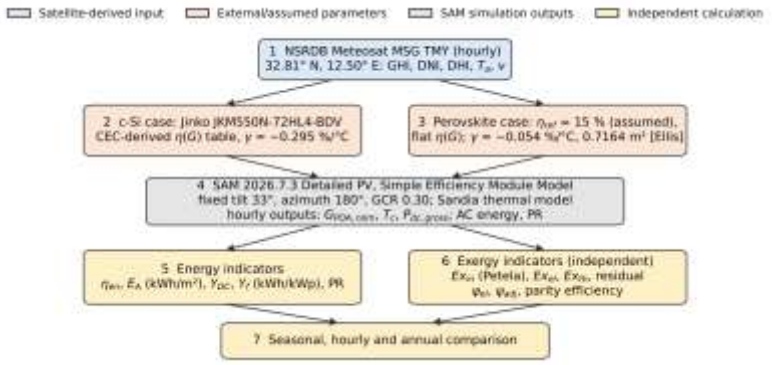

Fig. 2. Study workflow, color-coded by data type: satellite-derived input, external or assumed module parameters, SAM simulation outputs, and independently calculated indicators.

4. Results

4.1. Seasonal Energy and Exergy Performance

TABLE IV summarizes the seasonal results. On an area basis, c-Si outperforms perovskite in both seasons. Its energy efficiency is higher by 4.89 percentage points in summer and 5.67 percentage points in winter, and its ψ_{adj} by 5.26 and 6.07 percentage points. The approximate ψ_{el} gaps are similar (about 5.3 and 6.1 percentage points) because $Ex_{\mathrm{th}}/Ex_{\mathrm{in}}$ is common to both cases. The seasonal sensitivity is reversed. Between winter and summer, c-Si energy efficiency falls by 0.90 percentage points (4.5 relative percent), the approximate ψ_{el} falls by about 4 relative percent, and ψ_{adj} falls by 4.1 relative percent, while mean daytime cell temperature rises from 28.0 °C to 42.2 °C (maximum 67.7 °C). Perovskite energy efficiency falls by only 0.12 percentage points (0.8 relative percent), and its ψ_{adj} is marginally higher in summer (11.78%) than in winter (11.70%). The implied POA irradiation in TABLE IV is identical for both technologies, confirming a common radiative input.

TABLE IV. Seasonal module-level indicators (gross DC basis unless stated)

Indicator	c-Si summer	c-Si winter	Perovskite summer	Perovskite winter
Energy efficiency η_{en} (%)	18.96	19.86	14.07	14.19
Electrical exergy efficiency ψ_{el} (%), approx.[a]	20.4	21.3	15.1	15.2
Thermal-loss-adjusted indicator ψ_{adj} (%)[b]	17.04	17.77	11.78	11.70
$Ex_{\mathrm{th}}/Ex_{\mathrm{in}}$ (%), approx.[a]	3.3	3.5	3.3	3.5
$Ex_{\mathrm{th}}/Ex_{\mathrm{el}}$ (%)[b]	16.4	16.5	22.1	23.1
Gross DC energy per module area E_{A} (kWh/m²)	121.8	88.8	90.4	63.4
Gross DC specific yield Y_{DC} (kWh/kWp)	571	416	602	423
AC performance ratio PR (–)	0.82	0.86	0.86	0.87
Implied POA irradiation $E_{\mathrm{A}}/\eta_{\mathrm{en}}$ (kWh/m²)[a]	642.4	447.1	642.5	446.8

[a] Approximate reconstruction from published values using the Petela factor at seasonal mean daytime temperature (Section 3.4), or, for the last row, the ratio of two published values; [b] value published in the source analysis.

4.2. Hourly Performance on the Two Selected Days

For c-Si on 17 July (Fig. 3), the energy efficiency decreases from 20.2% in the early morning to 18.7% at 13:00, when the cell temperature reaches 51.4 °C. Over the same interval, ψ_{adj} decreases far more steeply, from 21.4% to 15.2%. Under the model, the larger midday dip of ψ_{adj} reflects the subtracted convective term of (6)–(7), which grows approximately with $(T_c - T_0)^2$ and with wind speed. The temperature response of the electrical exergy efficiency is a separate matter: hour by hour, ψ_{el} equals η_{en} divided by a Petela factor that varies by less than 0.5% over the day, so ψ_{el} follows the modest decline of η_{en} and stays near 20% at 13:00 (an approximate value, since the hourly ambient temperature was not available). The difference between this value and ψ_{adj} suggests a convective term of roughly 5% of the incident exergy rate at 13:00 on 17 July. In the early morning and late afternoon ψ_{adj} exceeds η_{en}, because radiation exergy is about 7% lower than radiation energy and Ex_{th} vanishes as T_c approaches T_0. This is consistent with the diurnal pattern reported by Pandey *et al.* [7]. Perovskite energy efficiency stays nearly constant (14.0–14.3%), while its ψ_{adj} follows the same pattern at a lower level (minima 10.2% in summer and 11.9% in winter).

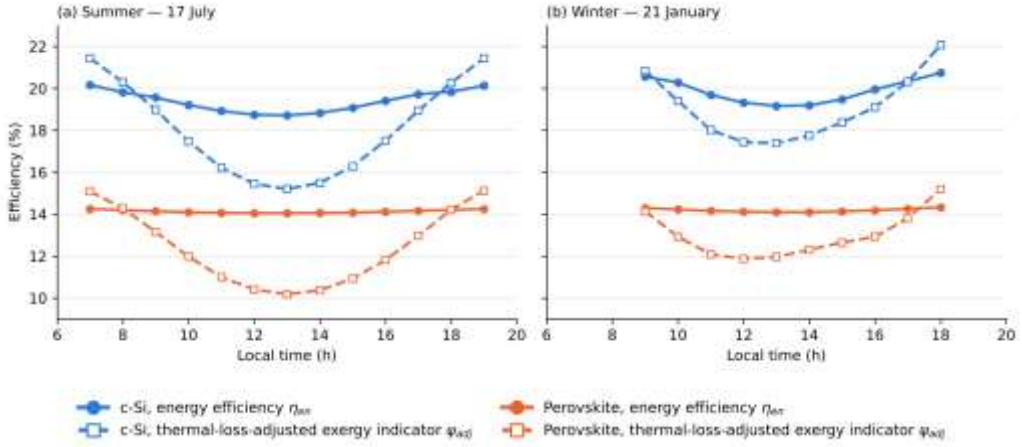

Fig. 3. Hourly energy efficiency (solid) and thermal-loss-adjusted exergy indicator ψ_{adj} (dashed) for the c-Si and perovskite cases on (a) 17 July and (b) 21 January. Data reproduced from the source analysis with the legend relabeled to (10); time-zone convention undocumented.

4.3. Exergy Budget and Thermal Exergy Transfer

Fig. 4 decomposes the exergy budget of the control volume of Section 3.4: the input is the exergy of nominal POA irradiance G (before shading, soiling, and reflection); the product is gross DC electrical exergy, generated from G_{eff} and evaluated before the 4.44% DC losses; and the bars show the approximate ψ_{el} and Ex_{th}/Ex_{in} (TABLE IV), a soiling share, and the unallocated exergy residual of (8). The plotted 5% soiling share is an accounting approximation. It assumes that the 5% irradiance loss carries the same exergy-to-energy ratio as the incident radiation, and it was not reconstructed from hourly irradiance streams before and after soiling. Soiling is counted only once: the soiling share is subtracted from the residual of (8) and appears nowhere else in the budget.

The modeled convective exergy transfer is about 3.3–3.5% of the input and, with identical modeled cell temperatures, the same per unit area for both technologies; it nevertheless represents a larger fraction of the useful output for perovskite (22–23% of Ex_{el}) than for c-Si (about 16%). After the soiling share, the unallocated exergy residual is about 70–71% of the input for c-Si and about 76% for perovskite. The available results do not quantify the contributions to this residual separately. Its size therefore does not by itself show which loss mechanism dominates, nor whether cell-level redesign or module cooling offers the larger improvement.

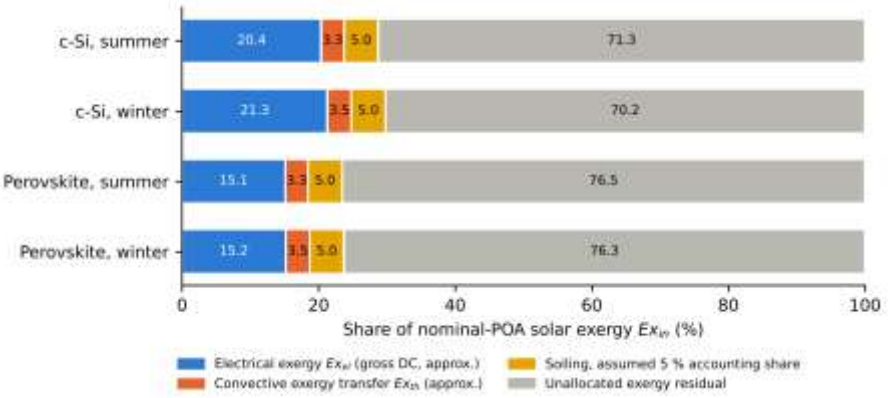

Fig. 4. Seasonal exergy budget relative to the exergy of nominal POA irradiance, replotted from TABLE IV. Electrical exergy (gross DC) and convective exergy are approximate reconstructions; the 5% soiling share is an assumed accounting approximation; the remainder is the unallocated exergy residual of (8).

4.4. Annual Specific Yield and Break-Even Efficiency

Fig. 5 compares area-normalized and capacity-normalized seasonal gross DC output. c-Si delivers 34.7% more energy per square metre in summer, whereas the perovskite case delivers about 5.4% more per installed kWp in summer (602 versus 571 kWh/kWp) and 1.7% more in winter (423 versus 416 kWh/kWp).

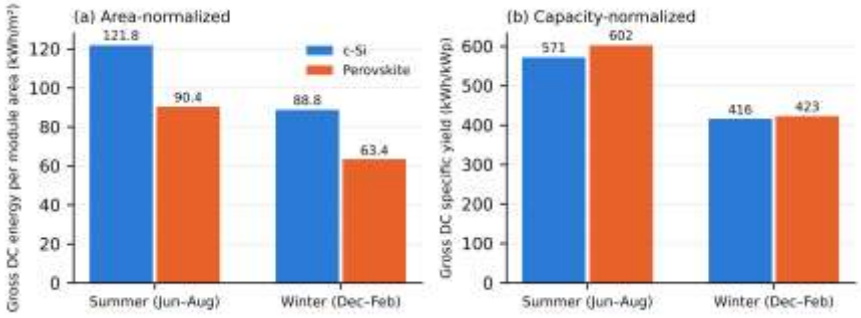

Fig. 5. Seasonal gross DC output normalized (a) by module area and (b) by installed DC capacity (values from TABLE IV).

c-Si leads per square metre because area-based output scales with the rated power density (213.2 versus 150 W/m²); perovskite leads per kWp because capacity normalization removes the rating and leaves the fraction of it delivered under Sabratha conditions (Section 5.1).

The source analysis also reports annual specific yields of 1,903 kWh/kWp for perovskite and 1,840 kWh/kWp for c-Si (a relative difference of 3.42%), and annual AC performance ratios of 0.86 and 0.83 (TABLE V). Each is normalized by its array's installed DC capacity, but the SAM output variable is undocumented and no annual export was available, so their basis (gross module DC, net array DC, or final AC) cannot be verified and the PR values cannot be recomputed. One consistency check is available. SAM defines its summary metric "energy yield" as annual AC energy divided by DC nameplate capacity [29]. If the reported values are this metric, dividing each by its PR gives nearly equal reference yields (about 2,215 kWh/kWp), as two arrays with identical geometry and weather should have. This agreement is consistent with, but does not prove, an AC basis. The annual values are therefore reported as stated, with an unconfirmed basis, and are not used in the comparisons.

TABLE V. Reported annual indicators (output basis unconfirmed) and conditional parity efficiency

Indicator	c-Si	Perovskite	Basis
Annual specific yield (kWh/kWp)	1,840	1,903	As reported; output basis unconfirmed
Annual AC performance ratio PR (–)	0.83	0.86	As reported; not recomputed
Parity reference efficiency η^*, summer (%)	–	≈20.2	Eq. (12), seasonal gross DC
Parity reference efficiency η^*, winter (%)	–	≈21.0	Eq. (12), seasonal gross DC

Applying (12) to the seasonal values in TABLE IV gives $\eta^* = 15\% \times 18.96/14.07 \approx 20.2\%$ in summer and $15\% \times 19.86/14.19 \approx 21.0\%$ in winter, compared with 21.32% for c-Si. These values rest on three conditions: common incident irradiance, common modeled thermal exergy per unit area, and perovskite DC output proportional to its reference efficiency. The annual threshold of 20.5% reported in the source is not included, because no traceable annual gross DC data on a common basis were available. The gap between 21.32% and η^*, about 1.1 percentage points in summer and 0.3 percentage points in winter, measures the net modeled advantage of the perovskite module's per-kWp derating behavior. These thresholds are conditional on the identical thermal model, the flat perovskite efficiency profile, and the absence of degradation.

5. Discussion

5.1. Area-Based Performance Versus Capacity-Normalized Yield

The two normalizations answer different questions and are kept distinct. Area-based indicators measure how much of the incident resource a module surface converts and are governed mainly by the reference efficiency (ratio 1.42), so c-Si leads clearly. Capacity-normalized yield measures how much energy each rated kilowatt delivers and is governed by the ratio η_{en}/η_{ref}, which equals 0.889 for c-Si and 0.938 for perovskite in summer, and 0.932 and 0.946 in winter. Soiling, transposition, reflection, and the thermal model are common to both arrays. The modeled module-specific factors are therefore the temperature coefficient and the relative irradiance–efficiency profile. Between 400 and 800 W/m² the c-Si profile lies 0.6–1.0% above its reference value, whereas the perovskite profile is flat. The irradiance effect thus works in favor of c-Si, and the per-kWp advantage of the perovskite case is attributable to its smaller temperature coefficient net of this opposing effect. The two contributions cannot be separated quantitatively without the hourly data. For equal capacity the perovskite array needs 42% more module area, so no cost or land advantage is implied.

5.2. Interpretation of Temperature Effects

The seasonal contrast follows from a temperature coefficient about five times larger for c-Si. Two points qualify the exergy interpretation. First, ψ_{el} tracks η_{en} almost exactly, so electrical exergy efficiency adds little beyond energy efficiency when only electricity is the product. The stronger temperature sensitivity of ψ_{adj} arises from the subtraction of Ex_{th}, not from the electrical output. Second, Ex_{th} in (6) depends on the wind correlation and on the use of T_c rather than a measured surface temperature. Because Ex_{th} scales linearly with h_c, a first-order calculation from the Ex_{th}/Ex_{in} shares in TABLE IV (0.3 × 3.3–3.5%) shows that a ±30% change in the correlation would shift ψ_{adj} by about ±1.0 percentage point in both seasons, without affecting η_{en}, ψ_{el}, or η^*.

5.3. Model Limitations and Validation Needs

The main limitations and their likely direction are as follows. (i) The satellite-derived TMY carries bias and random error relative to ground data; since both arrays share it, it affects absolute yields more than the comparison. (ii) No local field validation was possible. (iii) The common thermal model ignores the efficiency dependence of module temperature; the less efficient perovskite module would run slightly hotter, raising its Ex_{th} and lowering ψ_{adj}, with little effect on output given $\gamma = -0.054$ %/°C. (iv) The flat perovskite low-irradiance response is assumed; a declining response would lower

perovskite yield, especially in winter, and raise η^*. (v) Monofacial operation understates the yield of the bifacial c-Si module and may narrow or reverse the perovskite per-kWp advantage. (vi) Soiling is fixed at 5%; a seasonal profile would change absolute efficiencies and could shift η^* slightly (Section 3.5). (vii) Degradation is excluded, although Ellis *et al.* observed a loss of about 3 percentage points in efficiency over one year [13], so the results describe initial performance. (viii) The annual output basis is unconfirmed (Section 4.4). Validation requires co-located measurements in Libya of POA irradiance, back-surface temperature, wind, and DC power for both technologies, together with the SAM project and hourly exports.

6. Conclusion

An hourly SAM-based energy and exergy comparison of a TOPCon c-Si module and a modeled commercial-size perovskite module was carried out for two hypothetical fixed-tilt arrays in Sabratha, Libya. Within the stated assumptions: (1) Per unit module area, c-Si reaches higher energy efficiency (18.96–19.86%) and approximate electrical exergy efficiency (about 20.4–21.3%) than perovskite (14.07–14.19% and about 15.1–15.2%). (2) The modeled perovskite efficiency is nearly insensitive to summer heat. Its energy efficiency changes by 0.8 relative percent between seasons, against 4.5 relative percent for c-Si; consequently, the perovskite case produces about 5.4% more gross DC energy per installed kWp in summer and 1.7% more in winter, while c-Si produces more energy per square metre. (3) Under the model, the steep midday drop of the thermal-loss-adjusted indicator ψ_{adj} reflects the subtracted convective term, whereas the electrical exergy efficiency ψ_{el} closely follows energy efficiency. (4) Modeled convective exergy transfer is about 3.3–3.5% of incident exergy. The unallocated exergy residual is not resolved into separate mechanisms by the available results. (5) Under common irradiance and thermal assumptions, a perovskite module of this type would need a reference efficiency of about 20.2% to match c-Si in summer and 21.0% in winter. Generalization requires confirming the annual output basis, field data from Libya, efficiency-dependent thermal modeling, bifacial operation, and degradation.

Data Availability

Only the source manuscript (seasonal table, hourly and exergy-budget figures) was available; the SAM project, TMY file, and hourly and annual exports were not. Reproduction requires the SAM 2026.7.3 project for both arrays, the NSRDB Meteosat TMY file for 32.81° N, 12.50° E [23], and hourly exports of nominal POA irradiance, cell and ambient temperature, wind speed, gross and net DC power, and AC energy, plus the annual output variables.

References

[1] Y. Kassem, H. Camur, and O. A. M. Abughinda, "Solar energy potential and feasibility study of a 10MW grid-connected solar plant in Libya," *Eng. Technol. Appl. Sci. Res.*, vol. 10, no. 4, pp. 5358–5366, 2020, doi: 10.48084/etasr.3607.

[2] A. O. M. Maka, S. Salem, and M. Mehmood, "Solar photovoltaic (PV) applications in Libya: Challenges, potential, opportunities and future perspectives," *Clean. Eng. Technol.*, vol. 5, Art. no. 100267, 2021, doi: 10.1016/j.clet.2021.100267.

[3] M. Almaktar, A. M. Albreki, F. Mohamed, K. Yahya, and T. Hussein, "Performance evaluation of different solar photovoltaic technologies in Libya," in *Proc. 11th Int. Renewable Energy Congr. (IREC)*, 2020, pp. 1–5, doi: 10.1109/IREC48820.2020.9310421.

[4] Y. Nassar, H. El-Khozondar, S. Alsadi, N. Abuhamoud, and G. Miskeen, "Atlas of PV solar systems across Libyan territory," in *Proc. Int. Conf. Eng. MIS (ICEMIS)*, 2022, pp. 1–6, doi: 10.1109/ICEMIS56295.2022.9914355.

[5] A. S. Joshi, I. Dincer, and B. V. Reddy, "Thermodynamic assessment of photovoltaic systems," *Sol. Energy*, vol. 83, no. 8, pp. 1139–1149, 2009, doi: 10.1016/j.solener.2009.01.011.

[6] F. Sarhaddi, S. Farahat, H. Ajam, and A. Behzadmehr, "Exergetic optimization of a solar photovoltaic array," *J. Thermodyn.*, vol. 2009, Art. no. 313561, 2009, doi: 10.1155/2009/313561.

[7] A. Pandey, P. Pant, O. S. Sastry, A. Kumar, and S. K. Tyagi, "Energy and exergy performance evaluation of a typical solar photovoltaic module," *Therm. Sci.*, vol. 19, suppl. 2, pp. S625–S636, 2015, doi: 10.2298/TSCI130218147P.

[8] E. Cheikh, L. Mamadou, N. Ababacar, and A. Papa, "Outdoor performance analysis of a monocrystalline photovoltaic module: Irradiance and temperature effect on exergetic efficiency," *Int. J. Phys. Sci.*, vol. 10, pp. 351–358, 2015, doi: 10.5897/IJPS2015.4356.

[9] A. Sidibba, D. Ndiaye, D. Kobor, M. El Bah, and S. Bouhamady, "Energy and exergy analysis of a solar photovoltaic module performance under the Sahelian environment," *Int. J. Phys. Sci.*, vol. 13, pp. 196–205, 2018, doi: 10.5897/IJPS2018.4739.

[10] A. K. Jena, A. Kulkarni, and T. Miyasaka, "Halide perovskite photovoltaics: Background, status, and future prospects," *Chem. Rev.*, vol. 119, no. 5, pp. 3036–3103, 2019, doi: 10.1021/acs.chemrev.8b00539.

[11] E. Velilla, D. Ramírez, J.-I. Uribe, J. F. Montoya, and F. Jaramillo, "Outdoor performance of perovskite solar technology: Silicon comparison and competitive advantages at different irradiances," *Sol. Energy Mater. Sol. Cells*, vol. 191, pp. 15–20, 2019, doi: 10.1016/j.solmat.2018.10.018.

[12] M. Jošt *et al.*, "Perovskite solar cells go outdoors: Field testing and temperature effects on energy yield," *Adv. Energy Mater.*, vol. 10, no. 25, Art. no. 2000454, 2020, doi: 10.1002/aenm.202000454.

[13] H. Ellis, H. Müllejans, and E. D. Dunlop, "Outdoor measurements of perovskite modules," *Prog. Photovolt.: Res. Appl.*, 2026, doi: 10.1002/pip.70073.

[14] R. Petela, "Exergy of heat radiation," *J. Heat Transfer*, vol. 86, no. 2, pp. 187–192, 1964, doi: 10.1115/1.3687092.

[15] E. O. Ntor, H. Dandakouta, and A. M. Abioye, "Energy and exergy analysis to study the performance of a solar photovoltaic (PV) system with and without cooling system," *Nigerian J. Trop. Eng.*, vol. 17, no. 1, pp. 10–22, 2023, doi: 10.59081/njte.17.1.002.

[16] G. Huang, P. H. Arya, D. B. Ritzer, N. A. Alati, B. Abdollahi Nejand, U. W. Paetzold, and B. S. Richards, "Hybrid perovskite-photovoltaic and solar-thermal harvesting," *Adv. Sci.*, vol. 12, no. 42, Art. no. e09692, 2025, doi: 10.1002/advs.202509692.

[17] A. Richter, M. Hermle, and S. W. Glunz, "Reassessment of the limiting efficiency for crystalline silicon solar cells," *IEEE J. Photovolt.*, vol. 3, no. 4, pp. 1184–1191, Oct. 2013, doi: 10.1109/JPHOTOV.2013.2270351.

[18] F. Feldmann, M. Bivour, C. Reichel, M. Hermle, and S. W. Glunz, "Passivated rear contacts for high-efficiency n-type Si solar cells providing high interface passivation quality and excellent transport characteristics," *Sol. Energy Mater. Sol. Cells*, vol. 120, pp. 270–274, 2014, doi: 10.1016/j.solmat.2013.09.017.

[19] C. Battaglia, A. Cuevas, and S. De Wolf, "High-efficiency crystalline silicon solar cells: Status and perspectives," *Energy Environ. Sci.*, vol. 9, no. 5, pp. 1552–1576, 2016, doi: 10.1039/C5EE03380B.

[20] VDMA Photovoltaic Equipment, *International Technology Roadmap for Photovoltaics (ITRPV): 2025 Results*, 17th ed. Frankfurt am Main, Germany: VDMA, 2026.

[21] Jinko Solar Co., Ltd., "Tiger Neo N-type 72HL4-BDV 550–570 Watt," datasheet JKM550-570N-72HL4-BDV-F1-CN. [Online]. Available: https://www.jinkosolar.com/uploads/JKM550-570N-72HL4-BDV-F1-CN.pdf

[22] M. Sengupta, Y. Xie, A. Lopez, A. Habte, G. Maclaurin, and J. Shelby, "The National Solar Radiation Data Base (NSRDB)," *Renew. Sustain. Energy Rev.*, vol. 89, pp. 51–60, 2018, doi: 10.1016/j.rser.2018.03.003.

[23] National Laboratory of the Rockies, "NSRDB API: Meteosat Prime Meridian TMY (PSM v4)." [Online]. Available: https://developer.nrel.gov/docs/solar/nsrdb/ (accessed Nov. 22, 2026).

[24] *System Advisor Model (SAM)*, Version 2026.7.3. Golden, CO, USA: National Laboratory of the Rockies, 2026. [Online]. Available: https://github.com/NatLabRockies/SAM

[25] P. Gilman, "SAM photovoltaic model technical reference," National Renewable Energy Laboratory, Golden, CO, USA, Tech. Rep. NREL/TP-6A20-64102, 2015.

[26] D. L. King, W. E. Boyson, and J. A. Kratochvil, "Photovoltaic array performance model," Sandia National Laboratories, Albuquerque, NM, USA, Rep. SAND2004-3535, 2004.

[27] J. A. Duffie and W. A. Beckman, *Solar Engineering of Thermal Processes*, 4th ed. Hoboken, NJ, USA: Wiley, 2013.

[28] *Photovoltaic System Performance—Part 1: Monitoring*, IEC 61724-1:2021, International Electrotechnical Commission, Geneva, Switzerland, 2021.

[29] National Laboratory of the Rockies, "Energy yield (kWh/kW)," *SAM Help*. [Online]. Available: https://samrepo.nlr.gov/help/mtp_kwhkwyear1.html